# High force 10 kN piezoresistive silicon force sensor with output independent of force distribution

R.A.F. Zwijze, R.J. Wiegerink, G.J.M. Krijnen, J.W. Berenschot, M.J. de Boer, M.C. Elwenspoek
MESA+ Research Institute, University of Twente, P.O.Box 217, 7500 AE Enschede,
The Netherlands, Fax: x31-53-4893343, Email: A.F.Zwijze@el.utwente.nl

## Abstract

A silicon force sensor is realized in which the force is measured by compressing a meander shaped polysilicon strain gage. A second gage which is not loaded, is used for temperature compensation, for compensation of bending and stretching stresses in the chip and for common changes in zero load resistor values. It is shown that the output of the bridge is a linear function of the force and is independent of the force distribution on the chip. By measuring the resistance change along both gages, the force distribution on the chip can be determined so that it can be detected whether the sensor has an oblique load or not. The production process of the chip is simple and robust. A package is designed to apply the load. Results on hysteresis experiments are performed at four temperatures between 25 °C and 47 °C. The hysteresis measurement at room temperature is in close agreement with finite element calculations. The maximum hysteresis error is within ±0.14 % of the full-scale output (fso). Creep was tested by loading it five times. It follows that creep is smaller than 0.01 % of the fso. The total error including the interpolation error is within ±0.23 %.

**Keywords:** silicon load cell, silicon force sensor, creep, hysteresis

## 1. Introduction

Load cells are force sensors which are used in weighing equipment. Most conventional load cells are made from stainless steel or aluminum (see figure 1). Its deformation under a load is measured with metal strain gages. Relative high hysteresis and creep limit the accuracy of these load cells. To minimize these effects, expensive high-grade steels like $CuBe_2$, $AlMg_3$ and $TiAl_6V_4$ [2] and labor-intensive fabrication methods are required. To overcome these problems silicon is a good alternative. In [2] creep recovery experiments on metals and non-metals are presented. It shows that for silicon after 15 minutes of recovery, only 0.005-0.01% of the original deformation has not been recovered. The paper also shows that sapphire and germanium have better creep characteristics. In addition to the excellent mechanical characteristics of silicon, batch fabrication of silicon potentially offers low production costs. In this paper, a silicon load cell with polysilicon (poly-Si) strain gages is presented for loads up to 10 kN (1000 kg).

figure 1: Load cell of the cantype (photograph taken from [1]).

Mostly, strain gages are strained such that the maximum strain and the current are in the same direction, to obtain maximum sensitivity (longitudinal piezoresistive effect). Compression of strain gages, i.e. strain and current are perpendicular to each other is observed very little in literature (transverse piezoresistive effect). However, in [3] a pressure sensor is presented in which the monocrystalline strain gages are compressed by a boss which is attached to a membrane. The membrane and boss deflect due to the applied pressure. In [4] a metal force sensor is described in which a zeranin (88 Cu, 7 Mn, 1 Ge) strain gage is place on a hardened steel plate. A plate on which the maximum force of 500 kN is applied compresses this gage. Within a deviation of 3 %, the resistance change of the gage is independent of the force distribution. Hysteresis is within 0.1 % of the full-scale output (fso), non-linearity within 0.2 % of the fso and creep after 30 minutes within 0.17 % of the fso. In this paper a similar sensor is presented. New in the design is that it is made of silicon, it is compensated for the temperature coefficient of resistivity, for in plane stretching and bending stresses in the chip and for common changes in zero load resistor values. Besides, the force distribution can be measured so that it can be detected whether the sensor has an oblique load or not. A thorough analytical analysis is performed to describe the behavior of the sensor. Also a two-dimensional finite element model is built that is able to accurately predict the sensitivity of the sensor. Finally, the realization and measurements are treated.

## 2. Layout

In figure 2 a top and cross-sectional view of the 10 mm by 10 mm silicon chip is shown. Two poly-Si strain gages are deposited on it. Gage 1 is placed on top of the chip and is directly loaded/compressed with pressing blocks that pass on the applied force. The force distribution along gage 1 does not need to be uniform as is shown in figure 3. Gage 2 is situated in grooves in the substrate, next to gage 1, and is not directly loaded. Gage 2 serves as a compensation resistance. It will be shown in section 3 that the ratio of resistances 1 and 2 is independent of the force distribution and is only a function of the total force.

Both resistances ( $R_1$ and $R_2$ ) are connected in series. Each resistance, is divided into 16 parts, so that the resistance change can be measured at 16 different places on the chip (see figure 4). By doing this the force distribution on the chip can be determined From this information it can be decided whether the force is applied perpendicular to the load cell or not. For both $R_1$ and $R_2$ the next equations are valid:

$$R_1 = \sum_{s=1}^{16} R_1^s \ , \quad R_2 = \sum_{s=1}^{16} R_2^s \quad \text{and} \quad I = \frac{V_s}{R_1 + R_2} \ , \tag{1}$$

where $V_s$ is the supply voltage and $I$ the current going through both resistances.

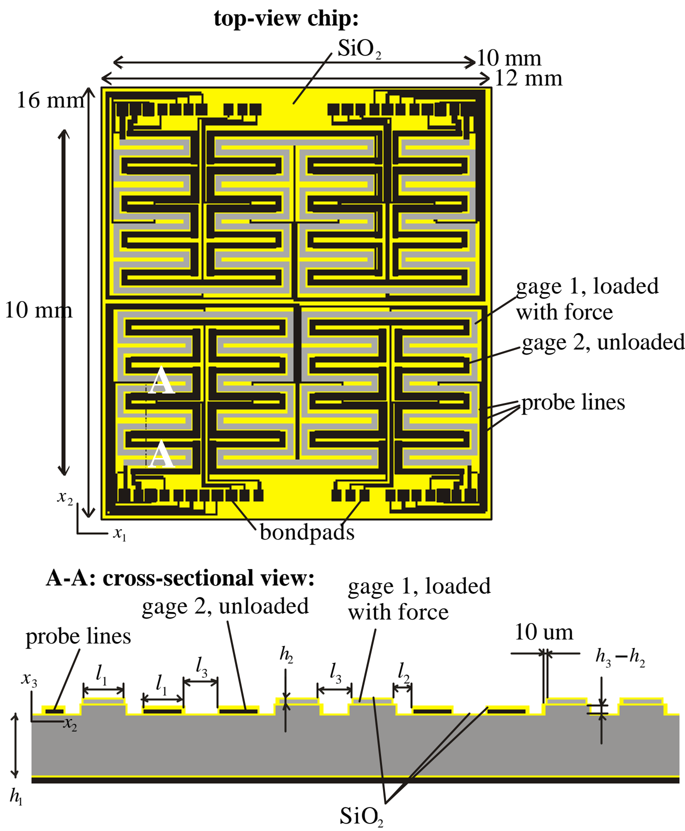

figure 2: Schematic layout chip with poly-Si strain gages.

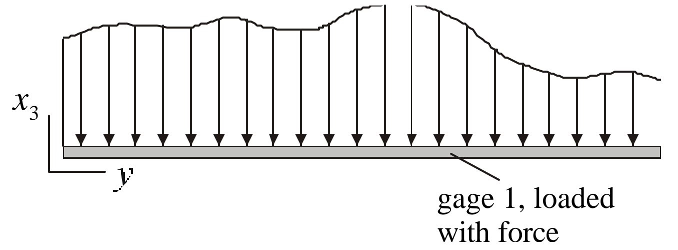

figure 3: Force distribution along strain gage 1.

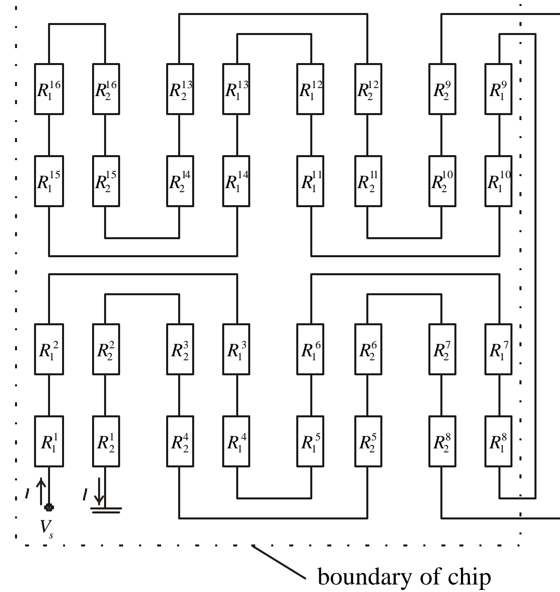

figure 4: Electrical equivalent of sensor structure.

## 3. Analytical theory

It is supposed that in the directions $x_1$, $x_2$ and $x_3$ (shown in figure 2) both strain gages are mainly subjected to three normal stresses and their corresponding strains. Although poly-Si shows the shear piezoresistance effect [5], shear strains are not considered here, because it will be shown with finite element simulations that they are small compared to the normal strains. It

is noted that for p-type doping levels between $5 \cdot 10^{18}$ cm$^{-3}$ and $1 \cdot 10^{20}$ cm$^{-3}$ and for a stress applied at 45° to the current flow, the shear gauge factor varies between 9 and 13. The normal strain $\varepsilon_{33}$ is acting in the direction of the force ( $x_3$-direction). $\varepsilon_{11}$ and $\varepsilon_{22}$ are in-plane normal strains which are perpendicular to the force and which act in the directions $x_1$ and $x_2$ respectively. It follows that the relative changes in resistance of both gages are given by [6]:

$$\frac{dR_1(y)}{R_1(y)} = G_l(T(y))\varepsilon^1_{11}(y) + G_t(T(y))\left(\varepsilon^1_{22}(y) + \varepsilon^1_{33}(y)\right) + \beta T(y) \quad \text{and}$$

$$\frac{dR_2(y)}{R_2(y)} = G_l(T(y))\varepsilon^2_{11}(y) + G_t(T(y))\left(\varepsilon^2_{22}(y) + \varepsilon^2_{33}(y)\right) + \beta T(y)\,. \tag{2}$$

$G_l(T(y))$ and $G_t(T(y))$ are the longitudinal and transverse piezoresistive strain gauge factors which depend on the temperature $T(y)$ ([6],[7]). The parameter $y$ represents the coordinate along both strain gages (see figure 3). At the entrance of a gage $y$ equals 0, at the end $y = L$ where $L$ is the total length of a gage. $\beta$ is the temperature coefficient of resistance. $\varepsilon^1_{jj}(y)$ and $\varepsilon^2_{jj}(y)$ ( $j$ =1,2,3) are the normal strains at position $y$ in gages 1 and 2 respectively.

In working out the analytical theory it is more convenient to uses stresses, instead of strains. Therefore, (2) is written as

$$\frac{dR_1(y)}{R_1(y)} = \pi_l(T(y))\sigma^1_{11}(y) + \pi_t(T(y))\left(\sigma^1_{22}(y) + \sigma^1_{33}(y)\right) + \beta T(y) \quad \text{and}$$

$$\frac{dR_2(y)}{R_2(y)} = \pi_l(T(y))\sigma^2_{11}(y) + \pi_t(T(y))\left(\sigma^2_{22}(y) + \sigma^2_{33}(y)\right) + \beta T(y)\,. \tag{3}$$

$\pi_l(T(y))$ and $\pi_t(T(y))$ are the longitudinal and transverse piezoresistive stress gauge factors. $\sigma^1_{jj}(y)$ and $\sigma^2_{jj}(y)$ ( $j$ =1,2,3) are the normal stresses in gages 1 and 2 respectively. In case one grain is considered which has an anisotropic homogeneous structure, then $\pi_l(T(y))$ and $\pi_t(T(y))$ are related to $G_l(T(y))$ and $G_t(T(y))$ by the compliance coefficients $S_{ij}$ [8]:

$$G_d = 1 - \sum_{j=1}^{6} \frac{S_{ij}}{S_{ii}}(1 - \delta_{ij}) + \frac{\pi_d}{S_{ii}}\,, \tag{4}$$

where $i = 1$ and $d = l$ for longitudinal strain, and $i = 2$ and $d = t$ for transverse strain. $S_{ij}$ can be calculated for an arbitrary direction using the following equations:

$$S_{ij} = S_{12} + (S_{11} - S_{12} - \frac{1}{2}S_{44})(l_i^2 l_j^2 + m_i^2 m_j^2 + n_i^2 n_j^2) \quad \text{and}$$

$$S_{ii} = S_{11} + (S_{44} + 2S_{12} - 2S_{11})(l_i^2 m_i^2 + l_i^2 m_i^2 + m_i^2 n_i^2)\,. \tag{5}$$

$l_i$, $m_i$ and $n_i$ are the direction cosines with respect to the principal axes.

In (3) $\sigma^i_{22}(y)$ and $\sigma^i_{33}(y)$ ( $i$ =1,2) consist of different contributions. First of all bending and stretching stresses (see figure 5). These stresses are present, because the surfaces of the silicon chip and pressing blocks which pass on the force do not exactly fit. Secondly, stresses caused by local deformation of the chip due to compression of gage 1 in the neighborhood of that location. The last mentioned stresses can be compared to the effect of a point force on a semi-infinite solid [9]. In a semi-infinite solid the stresses are independent of the boundary conditions imposed on the solid. As seen from figure 5, both bending and stretching stresses are the same in both gages at places situated next to each other. Then, by subtracting the relative changes of resistance of both strain gages, these stresses can be eliminated:

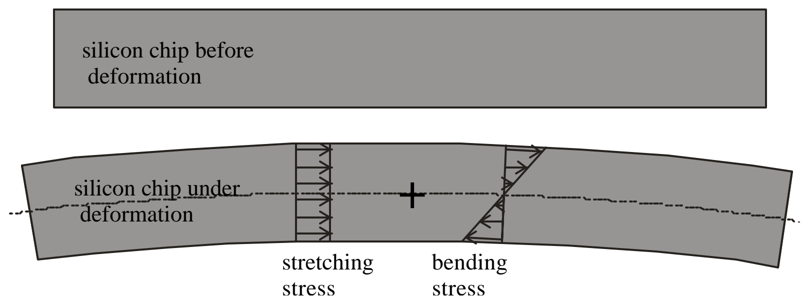


figure 5: Stretching and bending stresses in the silicon chip.

$$\frac{dR_1(y)}{R_1(y)}-\frac{dR_2(y)}{R_2(y)}=\boldsymbol{p}_l(T)\Delta\boldsymbol{s}_{11}^{nbs}(y)+\boldsymbol{p}_t(T)\left(\Delta\boldsymbol{s}_{22}^{nbs}(y)+\boldsymbol{s}_{33}^{1}(y)-\boldsymbol{s}_{33}^{2}(y)\right), \tag{6}$$

where

$$\Delta\boldsymbol{s}_{11}^{nbs}(y)=\boldsymbol{s}_{11}^{1}(y)-\boldsymbol{s}_{11}^{2}(y)\,,\quad \Delta\boldsymbol{s}_{22}^{nbs}(y)=\boldsymbol{s}_{22}^{1}(y)-\boldsymbol{s}_{22}^{2}(y)\,. \tag{7}$$

The index $nbs$ indicates no bending and stretching stresses. It is also seen that the temperature dependence $\boldsymbol{b}T(y)$ is eliminated. As the resistance of a gage is given by

$$\text{resistance}=\frac{\text{specific resistance* length}}{\text{width *height}}\,, \tag{8}$$

(2) can be written as

$$\frac{\dfrac{d\boldsymbol{r}_1(y)dy}{l_1h_2}}{\dfrac{\boldsymbol{r}_1(y)dy}{l_1h_2}}-\frac{\dfrac{d\boldsymbol{r}_2(y)dy}{l_1h_2}}{\dfrac{\boldsymbol{r}_2(y)dy}{l_1h_2}}=\boldsymbol{p}_l(T(y))\Delta\boldsymbol{s}_{11}^{nbs}(y)+\boldsymbol{p}_t(T(y))\left(\Delta\boldsymbol{s}_{22}^{nbs}(y)+\boldsymbol{s}_{33}^{1}(y)-\boldsymbol{s}_{33}^{2}(y)\right). \tag{9}$$

$\boldsymbol{r}_1(y)$, $\boldsymbol{r}_2(y)$ is the specific resistance in both gages at position $y$. $l_1$ en $h_2$ are the width and thickness of a gage (see figure 2). Integration of (9) gives

$$\int_{y=0}^{L}\left[\frac{\dfrac{d\boldsymbol{r}_1(y)dy}{l_1h_2}}{\dfrac{\boldsymbol{r}_1(y)L}{l_1h_2}}-\frac{\dfrac{d\boldsymbol{r}_2(y)dy}{l_1h_2}}{\dfrac{\boldsymbol{r}_2(y)L}{l_1h_2}}\right]L=\frac{1}{l_1}\int_{y=0}^{L}\left[\boldsymbol{p}_l(T(y))\Delta\boldsymbol{s}_{11}^{nbs}(y)+\boldsymbol{p}_t(T(y))\left(\Delta\boldsymbol{s}_{22}^{nbs}(y)+\boldsymbol{s}_{33}^{1}(y)-\boldsymbol{s}_{33}^{2}(y)\right)\right]l_1dy. \tag{10}$$

For small changes in $\boldsymbol{r}_1(y)$ and $\boldsymbol{r}_2(y)$, these parameters can be considered constant so that

$$\boldsymbol{r}_1(y)\approx\boldsymbol{r}_{1,0}\,,\quad \boldsymbol{r}_2(y)\approx\boldsymbol{r}_{2,0}\,. \tag{11}$$

Besides, it is assumed that the temperature is constant on the chip, so that

$$\boldsymbol{p}_l(T(y))\approx\boldsymbol{p}_l(T)\quad\text{and}\quad\boldsymbol{p}_t(T(y))\approx\boldsymbol{p}_t(T)\,. \tag{12}$$

Then, by using (11) and (12), (10) can be reduced to

$$\frac{\Delta R_1}{R_{1,0}}-\frac{\Delta R_2}{R_{2,0}}=\frac{F_{tot}\boldsymbol{p}_t(T)}{l_1L}+\frac{1}{l_1L}\int_{y=0}^{L}\left[\boldsymbol{p}_l(T)\Delta\boldsymbol{s}_{11}^{nbs}(y)+\boldsymbol{p}_t(T)\left(\Delta\boldsymbol{s}_{22}^{nbs}(y)-\boldsymbol{s}_{33}^{2}(y)\right)\right]l_1dy\,, \tag{13}$$

where

$$F_{tot}=\int_{y=0}^{L}\boldsymbol{s}_{33}^{1}(y)l_1dy\,,\quad \Delta R_1=\int_{y=0}^{L}\frac{d\boldsymbol{r}_1(y)}{l_1h_2}dy\,,\quad \Delta R_2=\int_{y=0}^{L}\frac{d\boldsymbol{r}_2(y)}{l_1h_2}dy\,,\quad R_{1,0}=\frac{\boldsymbol{r}_{1,0}L}{l_1h_2}\,,\quad R_{2,0}=\frac{\boldsymbol{r}_{2,0}L}{l_1h_2}\,. \tag{14}$$

In (13) and (14) the total force $F_{tot}$ is introduced, because integration of the mechanical stress along gage 1 yields the total force. As both gages are situated next to each other it applies that $R_{1,0}\approx R_{2,0}$ so that (13) reduces to

$$\frac{\left(R_{2,0}+\Delta R_1\right)-\left(R_{2,0}+\Delta R_2\right)}{R_{2,0}}\approx\frac{R_1-R_2}{R_2}=\frac{F_{tot}\boldsymbol{p}_t(T)}{l_1L}+\frac{1}{l_1L}\int_{y=0}^{L}\left[\boldsymbol{p}_l(T)\Delta\boldsymbol{s}_{11}^{nbs}(y)+\boldsymbol{p}_t(T)\left(\Delta\boldsymbol{s}_{22}^{nbs}(y)-\boldsymbol{s}_{33}^{2}(y)\right)\right]l_1dy\,. \tag{15}$$

Then, it is assumed that the influence of the border of the chip can be neglected. This assumption seems reasonable, because the gages are much smaller than the chip size. Besides, as bending and stretching stresses were already eliminated, it means that the chip can be considered as an unbent and unstretched medium with infinite in-plane dimensions (in-plane means perpendicular to the force). Therefore, the influence of a point force $F(y_i)$ at place $y_i$ on the resistance change of the gages, is independent of its position on the chip. Due to the linear material behavior of silicon, the stresses in the chip at some position $y$ can be calculated by adding the stresses due to all point forces. Therefore, the integral term in (13) can be written as

$$\frac{1}{l_1L}\int_{y=0}^{L}\left[\boldsymbol{p}_l(T)\Delta\boldsymbol{s}_{11}^{nbs}(y)+\boldsymbol{p}_t(T)\left(\Delta\boldsymbol{s}_{22}^{nbs}(y)-\boldsymbol{s}_{33}^{2}(y)\right)\right]l_1dy=\sum_{i=1}^{n}k(T)F(y_i)=k(T)\sum_{i=1}^{n}F(y_i)=k(T)F_{tot}\,, \tag{16}$$

where $k(T)$ is some constant that depends on the temperature. Combination of (15) and (16) gives

$$\frac{R_1}{R_2}-1=\Delta\left(\frac{R_1}{R_2}\right)=\left[\frac{\pi_t(T)}{l_1 L}+k(T)\right]F_{tot}=K(T)F_{tot}=K_1\left(1+\alpha_1(T-T_0)\right)F_{tot}\,. \tag{17}$$

$K(T)$ is the sensitivity coefficient at temperature $T$ and $K_1$ is the sensitivity coefficient at room temperature $T_0$. It consists of the longitudinal and transverse gauge factors. $\alpha_1$ is the temperature coefficient of sensitivity. This equation shows that the change in ratio of both resistances is only a function of the total force, which makes the load cell independent of the force distribution.

The force at one of the 16 areas on the chip is calculated from

$$F_{tot}^{s}=\frac{\Delta\left(\dfrac{R_1^s}{R_2^s}\right)}{\sum_{p=1}^{16}\Delta\left(\dfrac{R_1^p}{R_2^p}\right)}F_{tot}=\frac{\Delta\left(\dfrac{R_1^s}{R_2^s}\right)}{\sum_{p=1}^{16}\Delta\left(\dfrac{R_1^p}{R_2^p}\right)}\frac{\Delta\left(\dfrac{R_1}{R_2}\right)}{K(T)}\qquad s=1..16\,, \tag{18}$$

where equation (17) is used for elimination of the total force. $\Delta\left(R_1^s/R_2^s\right)$ is the change in resistance ratio at area $s$ on the chip.

## 4. Finite element model

In order to get a prediction of the constant $K_1$ in equation (17), a two-dimensional finite element model of the chip was built in Ansys (see figure 6). Plane42 elements were used with a plane stress restriction. The elastic constants correspond to a coordinate system in which <100> is the normal direction and in which the in-plane axes are oriented in <110> directions [10]. The mean pressure $\bar{p}$ is applied on top of gage 1 (the protuberances in figure 6). The pressure is given by

$$\bar{p}=\frac{F_{tot}}{l_1 L}=\frac{g m_{tot}}{l_1 L}\,, \tag{3-19}$$

where $m_{tot}$ is the total mass which is applied to the chip. The total mass is related to the total force $F_{tot}$ by the gravitational acceleration $g$ which equals 9.81 m/s$^2$. For two choiches of length $L$, the parameters are shown in table 1, respectively denoted by design 1 and design 2. A plot of the compression of the chip and the $\sigma_{22}$ and $\sigma_{33}$ stresses around gage 1 and 2 is shown in figure 7 for design 1. From the simulations it follows that exept for a small part at the boundary of the chip, in all gages the stresses are the same. Besides, as the stresses and strains are rather constant inside the gages, the numerical values of the stresses and strains in the center of a gage are shown in table 1. By using these values, the change in ratio $R_1/R_2$ can be calculated from

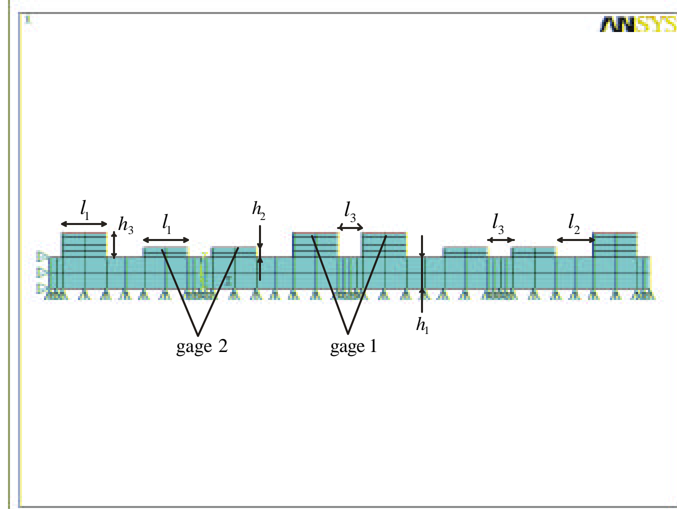


figure 6: Two-dimensional finite element model of chip.

$$\Delta\left(\frac{R_1}{R_2}\right)=G_l(T_0)\left(\varepsilon_{11}^1-\varepsilon_{11}^2\right)+G_t(T_0)\left(\varepsilon_{22}^1-\varepsilon_{22}^2+\varepsilon_{33}^1-\varepsilon_{33}^2\right)=K_1F_{tot}\,, \tag{20}$$

where equation (2) and (17) have been combined. The individual relative changes of resistance are also calculated for comparison to experiments. For both gages they are given by

$$\frac{\Delta R_1}{R_{1,0}}=G_l(T_0)\varepsilon_{11}^1+G_t(T_0)\left(\varepsilon_{22}^1+\varepsilon_{33}^1\right)=K_1^1F_{tot},\quad \frac{\Delta R_2}{R_{2,0}}=G_l(T_0)\varepsilon_{11}^2+G_t(T_0)\left(\varepsilon_{22}^2+\varepsilon_{33}^2\right)=K_1^2F_{tot}\,. \tag{21}$$

table 1: Parameters and output results of finite element simulations.

| parameter | design 1 | design 2 | parameter | design 1 | design 2 |
|---|---|---|---|---|---|
| $h_1$ [*m*m] | 380 | 380 | $s^2_{11}$ [MPa] | 0 | 0 |
| $h_2$ [*m*m] | 1.28 | 1.28 | $s^2_{22}$ [MPa] | 105.0 | 97.4 |
| $h_3$ [*m*m] | 3.58 | 3.58 | $s^2_{33}$ [MPa] | -0.0052 | -0.021 |
| $l_1$ [*m*m] | 91 | 91 | $s^2_{13}$ [MPa] | -0.050 | -0.22 |
| $l_2$ [*m*m] | 30 | 30 | $e^1_{11} \cdot 10^{-3}$ | 0.500 | 0.847 |
| $l_3$ [*m*m] | 30 | 205 | $e^1_{22} \cdot 10^{-3}$ | -0.551 | -0.013 |
| $L$ [*m*m] | 416984 | 254076 | $e^1_{33} \cdot 10^{-3}$ | -1.592 | -0.246 |
| $m_{tot}$ [kg] | 1000 | 1000 | $e^1_{13} \cdot 10^{-6}$ | -0.232 | -0.096 |
| $\overline{p}$ [GPa], | 0.259 | 0.424 | $e^2_{11} \cdot 10^{-3}$ | -0.039 | -0.036 |
| $s^1_{11}$ [MPa] | 0 | 0 | $e^2_{22} \cdot 10^{-3}$ | 0.621 | 0.576 |
| $s^1_{22}$ [MPa] | -187.5 | -379.8 | $e^2_{33} \cdot 10^{-3}$ | -0.226 | -0.210 |
| $s^1_{33}$ [MPa] | -259.4 | -426.0 | $e^2_{13} \cdot 10^{-6}$ | -0.632 | -0.028 |
| $s^1_{13}$ [MPa] | -0.018 | -0.0076 | $K_1 \cdot 10^{-5}$ [N$^{-1}$] | 0.2925 | 0.4793 |
| $s_{VM}$ [GPa] | 0.36 | 0.55 | $K^1_1(T) \cdot 10^{-5}$ [N$^{-1}$] | 0.2583 | 0.4477 |
| maximum compression [*m*m] | 0.42 | 0.52 | $K^2_1(T) \cdot 10^{-5}$ [N$^{-1}$] | -0.03414 | -0.03165 |

In [11] the gauge factors were experimentally determined for heavily doped boron diffused poly-Si resistors. The production of the chip which will be presented in section 5 is performed with the same process and in the same cleanroom. Therefore, the gauge factors presented in [11] are used in the calculations:

$$G_l(T_0) = 25 \text{ and } G_t(T_0) = -6 . \tag{22}$$

The maximum compression in the chip, maximum Von Mises stress $s_{VM}$ and sensitivity parameters $K_1$, $K_1^1$ and $K_1^2$ are shown in table 1. It follows that due to compression of the chip the pressing blocks will not touch gage 2, because $h_3 - h_2$ is larger than the maximum compression of the protuberances. Besides, the maximum value of the Von Mises stress indicates that there will probably be no rupture of the chip, because Peterson reports on a maximum tensile strength of 6.9 Gpa [12]. Clearly, it follows that $R_1$ increases and $R_2$ decreases.

## 5. Realization

The resistors are made from poly-Si and have to made electrically active by adding some dopant. Except for very high dopant concentrations, doping by diffusion does not guarantee adequate uniformity and repeatability in poly-Si films [13]. Uniformity of the doping concentration on a chip is important for a constant gauge factor across a chip, because the output signal has to be independent of the force distribution. Concerning the dopant type in poly-Si, it is preferred that boron is used, since n-type doping substances such as arsenic and phosphorus lead to segregation effects at the grain boundaries ([13],[14]), thereby reducing the stability. For boron no segregation is observed [14]. In [13] it is also reported that highly doped poly-Si layers may show a very low drift. The stability is explained from the very high free-carrier concentration, but also due to the high temperature treatment of the poly-Si film, which results in a stable crystallographic structure for the resistors. Experiments show that the resistance change of a poly-Si resistor at 200 ºC is only 0.00015 %/day. In [15] it is reported that poly-Si resistors are capable of realizing at least as high a level of long-term stability as may be expected from resistors in monocrystalline silicon, since surface effects only play a secondary role in device characteristics. Results with non-passivated resistors show that at a temperature of 125 ºC over a time period of 1000 hours, a drift of less than 0.5 % is obtained. The same paper concludes

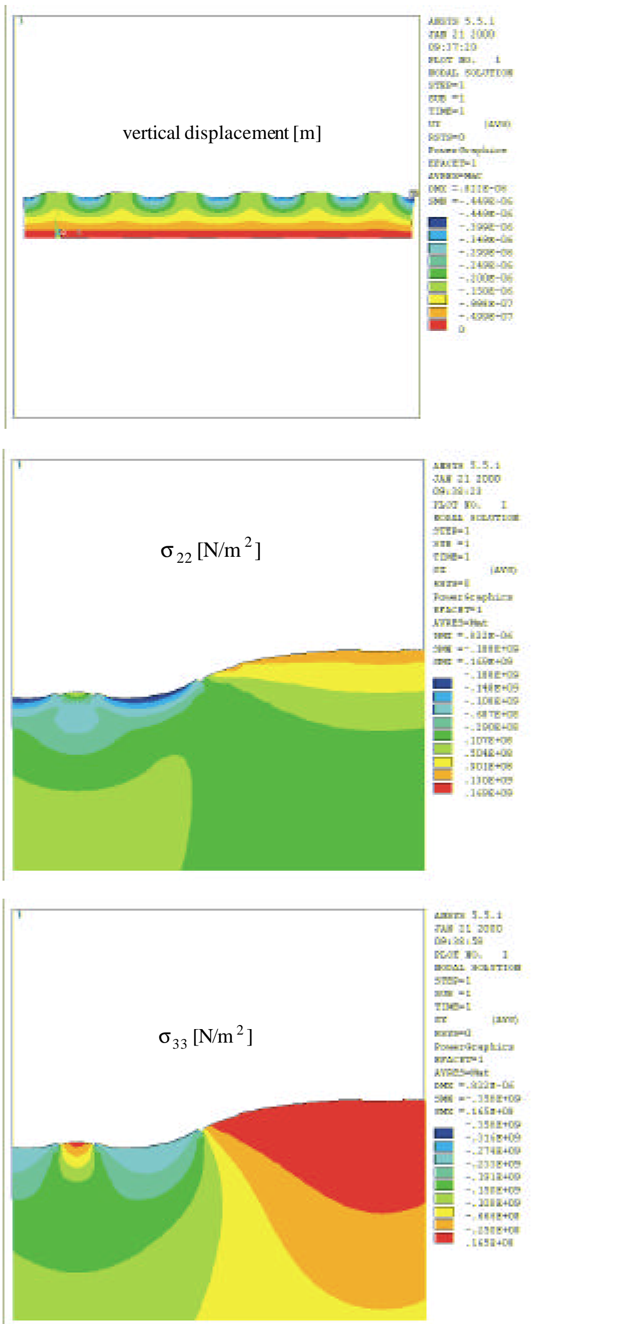


figure 7: Finite element results for chip with long gages: vertical displacement, $\sigma_{22}$ and $\sigma_{33}$.

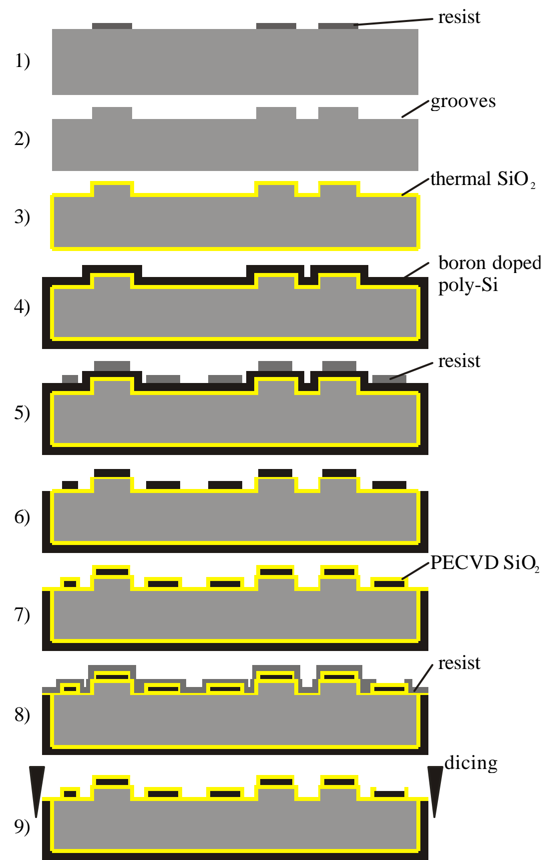


figure 8: Process scheme chip.

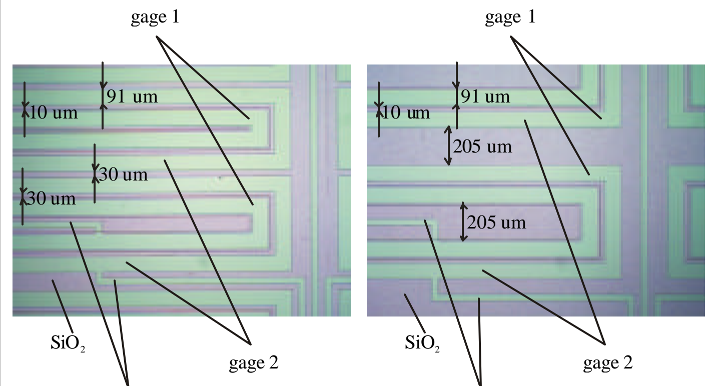


figure 9: Pictures of strain gages, design 1 (left) and design 2 (right).

that passivation with plasma-deposited $Si_3N_4$ will result in a corresponding improvement in drift characteristics. In [16] passivation of the resistors is done with both $SiO_2$ and $Si_3N_4$. Additional advantages are that these layers also serve as an antireflection coating and encapsulation during the recrystallization process. From the preceding considerations the choice was made to use a boron diffusion process. The doping level is high for this process ($\approx 10^{20}$ $cm^{-3}$). The process is relatively inexpensive to be carried out, because 20 wafers can be diffused at once.

The process scheme of the chip is shown in figure 8. First of all, in step 1 resist is patterned to define the grooves in which gage 2 will be deposited. Then, in step 2, 2.3 µm deep grooves are made by reactive ion etching (RIE) with a gas mixture of $O_2$, $CHF_3$ and $SF_6$. Hereafter, in step 3, a 0.7 µm thick layer of thermal silicon oxide is grown at 1150 °C. The amount of silicon consumed during this process is 44 % of the thermal oxide thickness [17]. Then, in step 4 a 1.28 µm thick poly-Si layer is grown. This process is directly followed by a boron diffusion process with boron nitride wafers to make the poly-Si electrically active [18]. Then, in step 5 resist is deposited to define the poly-Si strain gages. The poly-Si is etched by reactive ion etching using $SF_6$ gas (step 6). In step 7, a 0.7 µm thick PECVD silicon oxide layer is deposited for passivation of the resistors. Contrary to the first oxidation step, this step does not consume poly-Si. In this way stress concentrations at the surface between the first $SiO_2$ layer and the poly-Si are prevented. In step 8 resist is patterned to define the openings in the PECVD $SiO_2$ at the bondpads. Finally in step 9, this oxide is etched in BHF. Now, the wafers are ready for dicing which is also shown in step 9.

Pictures of the strain gages of the realized designs 1 and 2 are shown in figure 9. The production process is robust and under normal process conditions all chips will work properly.

## 6. Electronics

In order to determine the force distribution on the chip the resistance along 16 parts of both gages is determined. Besides, for the determination of the total force the total resistance of both gages has to be measured, which means that in total 34 measurements have to be performed. For this the electrical circuit shown in figure 10 was used. The four 16-channel analog multiplexers/demultiplexers are driven by the channels $\{SA_0..SA_3, SB_0..SB_3, SC_0..SC_3, SD_0..\ SD_3\}$ from the microcontroller. For example, for selecting resistances $R_1^8$ and $R_2^8$ the channels $\{A_7, B_7\}$ and $\{C_7, D_7\}$ must be selected. For resistances $R_1 = R_1^0$ and $R_2 = R_2^0$ channels $\{A_0, B_{15}\}$ and $\{C_0, D_{15}\}$ have to be selected. Now, the ratio of two resistances is given by dividing the voltages across these resistances:

$$\frac{R_1^s}{R_2^s} = \frac{IR_1^s}{IR_2^s} = \frac{V_1^s}{V_2^s} = \frac{V_{ZA} - V_{ZB}}{V_{ZC} - V_{ZD}}, \quad s = 0..16\ . \tag{23}$$

$\{V_1^s, V_2^s\}$ are voltages across part $s$ of gage 1 and 2 respectively. For $s = 0$ the total resistances are selected. $\{V_{ZA}, V_{ZB}, V_{ZC}, V_{ZD}\}$ are the voltages that are passed trough by the multiplexers. Clearly, the ratio is independent of current $I$.

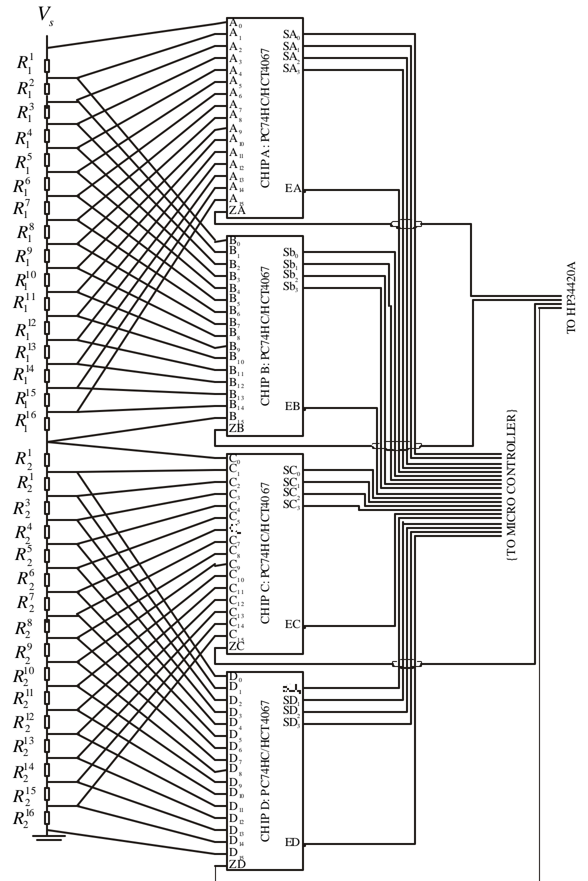


figure 10: Electrical circuit.

## 7. Measurements

The edge of the chip was glued with Araldit on a steel spring. Then, the spring was mounted in the package that is shown in figure 11. The pressing blocks are made from aluminum oxide. Due to the polishing of these blocks, the surface has become somewhat curved. Between the center and the brim of these blocks there is a height difference of about 900±100 nm which means that gage 1 will be compressed most in the center of the chip. On the spring, next to the chip, a platinum-sensing resistor (Pt100-element) is attached for measurement of the temperature. The sensor can measure temperatures from –70 °C to

+600 °C. In the fundamental interval from 0 to 100 °C the stability is ±0.05 %. By soldering a copper wire from the spring to the Pt100-element, it is expected that the temperature of the Pt100-element is equal to the temperature of the chip. The membrane that is attached to the cover, takes care of lateral forces and it puts a small preload on the chip (about 5 to 10 kg).

A test setup was realized to apply weights up to 1000 kg in steps of about 200 kg. The difference between the five 200 kg weights is within ±2.5 kg. However, important for the setup is not the exact mass of each weight, but repeatability in applying the weights. Exact calibration of load cells has to be done in institutes that are certified for this.

Then, hysteresis was tested at room temperature, which is at 24.5±0.1 °C. The resistance ratio $R_1/R_2$ as a function of the applied mass is shown in figure 12. It is seen that for zero loads $R_1/R_2$ is not equal to 1. There are three reasons for this. First of all, both resistances are not exactly equal. Secondly, the membrane of the package puts some preload on the chip. Thirdly, the arm of the test setup that applies the load to the package has a non-zero mass.

Hysteresis experiments were also performed at temperatures higher than room temperature. The results of all hysteresis experiments are shown as dots in figure 13. Interpolation of these results is done by considering the theoretical relation between $R_1/R_2$ and the total mass $m_{tot}$, equation (17). By also including temperature effects at zero load and the difference in zero load resistance for $R_1$ and $R_2$, it follows that this relation is in theory given by

$$\frac{R_1}{R_2} = K_0\left(1+\alpha_0(T-T_0)\right) + K_1\left(1+\alpha_1(T-T_0)\right)g m_{tot}, \quad (24)$$

where $K_0$ is the offset constant at zero load, $K_1$ the

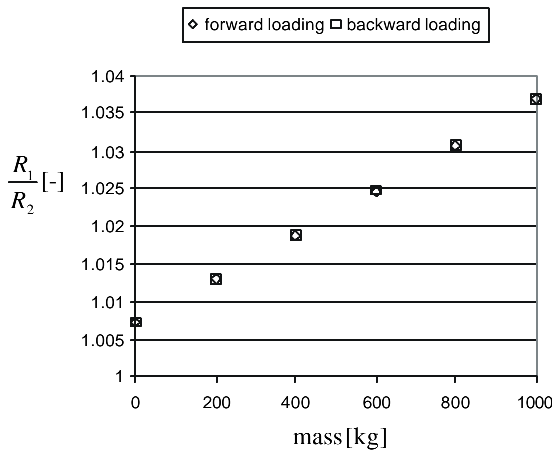


figure 12: Hysteresis at room temperature.

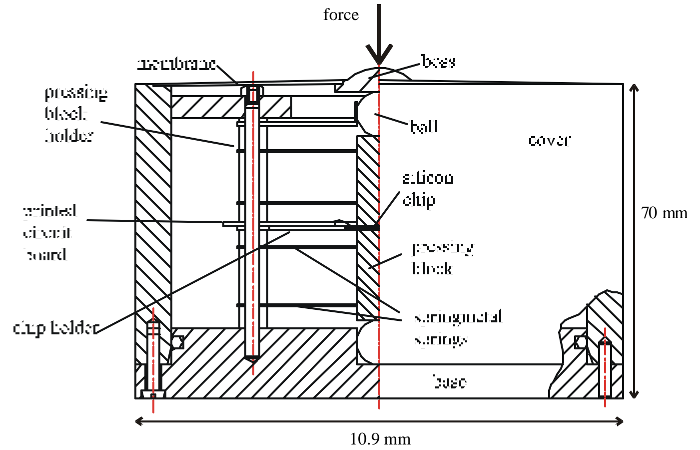


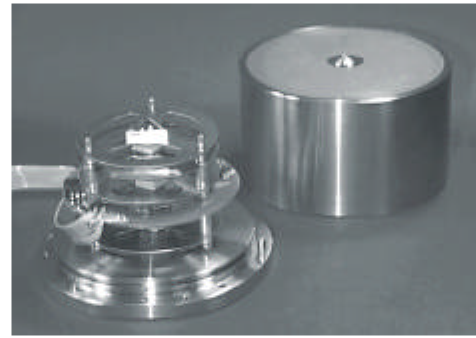

figure 11: Package.

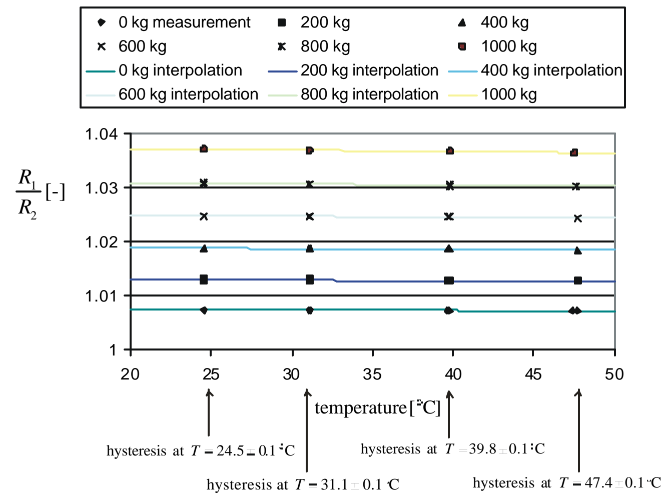


figure 13: Hysteresis measurements at different temperatures. The measurements include forward and backward loading.

sensitivity coefficient, $\boldsymbol{a}_0$ the temperature coefficient of the offset constant and $\boldsymbol{a}_1$ the temperature coefficient of the sensitivity constant. Interpolation of the measurements and constants $K_0, K_1, \boldsymbol{a}_0$ and $\boldsymbol{a}_1$ is done by using the program Statgraphics Plus 3.0. For $T_0 = 24.5\,°\mathrm{C}$ the next results are obtained:

$$K_0 = 1.0071\,, \quad \boldsymbol{a}_0 = -3.487 \cdot 10^{-6}\ °\mathrm{C}^{-1}\,,$$
$$K_1 = 0.3025 \cdot 10^{-5}\ \mathrm{N}^{-1}\,, \quad \boldsymbol{a}_1 = -832.4 \cdot 10^{-6}\ °\mathrm{C}^{-1}\,. \qquad (25)$$

By using these constants the interpolation error is within ±8.47 kg. It is remarkable that the sensitivity coefficient $K_1$ only deviates 3.4 % from the theoretical value ( $K_1$ ) obtained from the finite element calculations (see table 1). The temperature coefficient of sensitivity $\boldsymbol{a}_1$ corresponds to the temperature coefficient of the gauge factor given in [19]: $-1.3 \cdot 10^{-3}\ °\mathrm{C}^{-1}$ (longitudinal strain, p-type carrier concentration $10^{20}$ $\mathrm{cm}^{-3}$). However, it is noted that $\boldsymbol{a}_1$ is a function of the temperature coefficient of both the longitudinal and transverse gauge factors so that comparison is a bit difficult. Nevertheless, this value is much larger than for metal strain gages. For example, the temperature coefficient of the gauge factor of constantan is more than 7 times lower: $0.115 \cdot 10^{-3}\ °\mathrm{C}^{-1}$.

In order to obtain a better fit of the experimental results other interpolation formulas were tried. The best results were obtained for the next equation:

$$\frac{R_1}{R_2} = K_0\left(1 + \boldsymbol{a}_0(T - T_0)\right) + K_1\left(1 + \boldsymbol{a}_1(T - T_0)\right) g m_{tot} + K_2 m_{tot}^2\,. \qquad (26)$$

Now, the interpolation error is between ±2.25 kg (0.225 % of the fso). Equation (26) is drawn in figure 13, together with the data from the measurements. The hysteresis error was obtained by inserting the measured temperature and ratio $R_1 / R_2$ in interpolation polynom (26). From the calculated mass the real applied mass was subtracted. The result is shown in figure 15. The figure shows typical hysteresis plots. The figure also shows that at 400 kg, the measured mass is systematically underestimated. Probably, this means that the 200 kg weight which is put on when 400 kg has to be applied, is somewhat smaller in weight than the other 200 kg weights. By adding 1.5 kg to this weight this underestimation can be eliminated. Therefore, a better method for obtaining the real hysteresis is by subtracting the forward and backward absolute hysteresis error in figure 15. The result is shown in figure 16 and is called the relative hysteresis error. The figure shows that the relative hysteresis error is within ±1.38 kg (±0.138 % of the fso). Probably, most of this error is caused by slip of the pressing blocks on gage 1. In order to reduce the influence of this slip a top wafer has to be bonded on top of gage 1. Attempts were made to bond wafers on top of oxidized boron doped poly-Si layers which were chemically mechanically polished [20]. However, bonding appeared to be very bad. There are probably two reasons for this. First, of all it is believed that oxidation of the grain boundaries results in too much

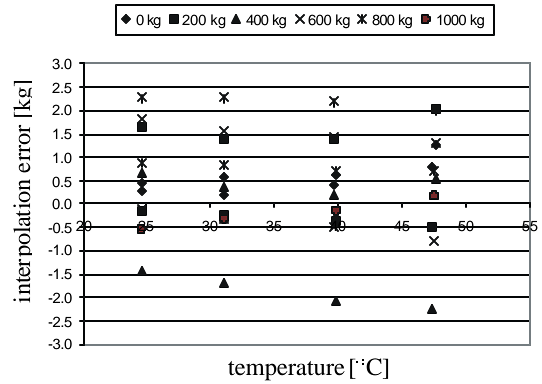

figure 14: Interpolation error for equation (26).

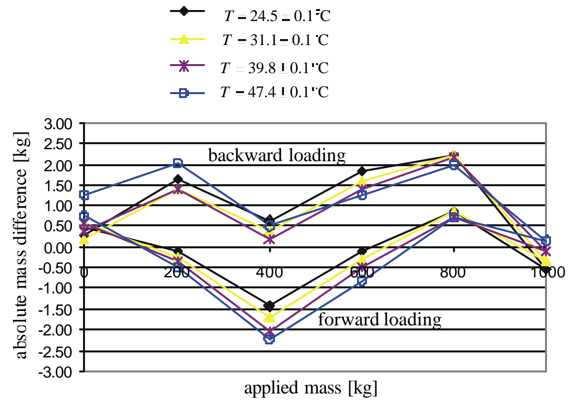

figure 15: Absolute hysteresis error.

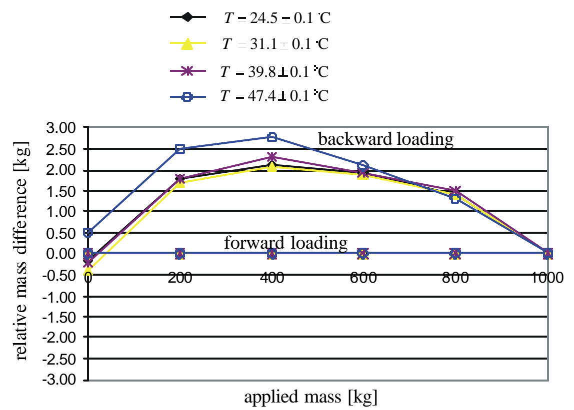

figure 16: Relative hysteresis error.

roughening so that bonding becomes impossible. Secondly, the diffusion equipment did not give uniform doping profiles, because the boron nitride wafers and the silicon wafers are placed somewhat oblique with respect to each other. Probably, SOI wafers with a highly doped mono crystalline silicon layer can be bonded to another wafer so that slip is reduced.

Then, creep was tested at 1000 kg. By using interpolation formula (26), the mass was determined as a function of time for 30 minutes. At 1000 kg, five creep experiments were performed to test repeatability of creep. At the same time the temperature was measured. Both results are shown in figure 17. It shows that creep is smaller than 0.1 kg (0.01 % of the fso) and is not influenced by the temperature. However, there is some non-repeatability in the measured mass for the first three loadings, giving a creep repeatability error which is within ±0.35 kg (±0.35 % of the fso). Again, it is believed that the non-repeatability is caused by slip of the pressing blocks on the chip.

The voltage change across gage 1 and 2 at room temperature is shown in figure 17. From these results the sensitivity coefficients as defined in (21) can be calculated:

$$K^1_{1,\text{experimental}} \approx \frac{V_1(m_{tot}=1000\,\text{kg})}{V_1(m_{tot}=0\,\text{kg})} - 1 = 0.1475\cdot 10^{-5}\ \text{N}^{-1} \text{ and } K^2_{1,\text{experimental}} \approx \frac{V_2(m_{tot}=1000\,\text{kg})}{V_2(m_{tot}=0\,\text{kg})} - 1 = -0.1500\cdot 10^{-5}\ \text{N}^{-1}. \quad (27)$$

Comparing these results to the theoretical results shown in table 1, it follows that $K^2_{1,\text{experimental}}$ is 4.4 times larger than $K^2_{1,\text{theoretical}}$. This can be explained from the fact that in the finite element calculations there is no bending and stretching of the chip due to the misfit between the surfaces of the chip and pressing blocks. This results in a small deformation of gage 2. Therefore, it is concluded that bending and stretching stresses have a significant contribution to the resistance changes of the gages. This means that it is important to use gage 2 for elimination of these stresses.

Finally, the force distribution was determined using equation (18). The result at 1000 kg is shown in figure 19. It is seen that the mean pressure is 3 times higher in the center than on the brim of the chip. The difference is explained from the curvature of the pressing blocks.

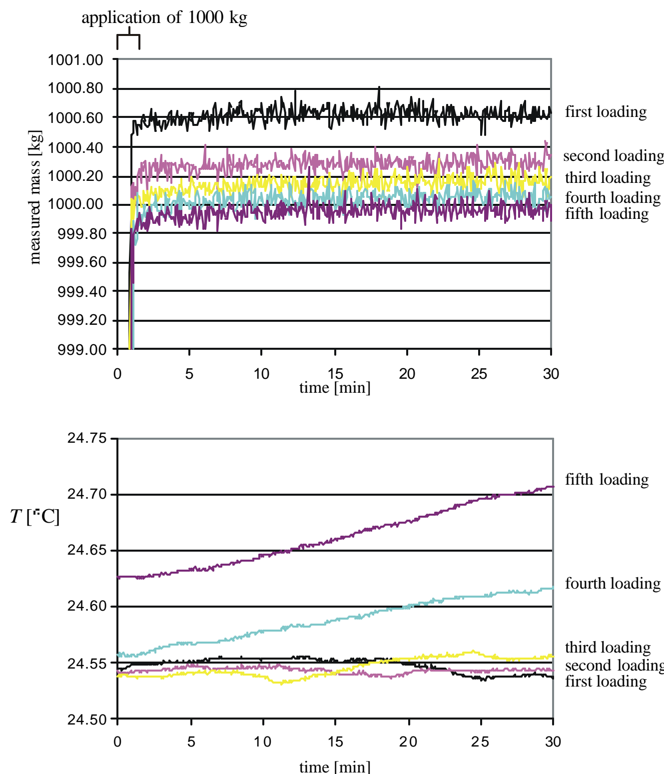

figure 17: Measured creep and temperature on application of a mass of 1000 kg, load cell is loaded five times.

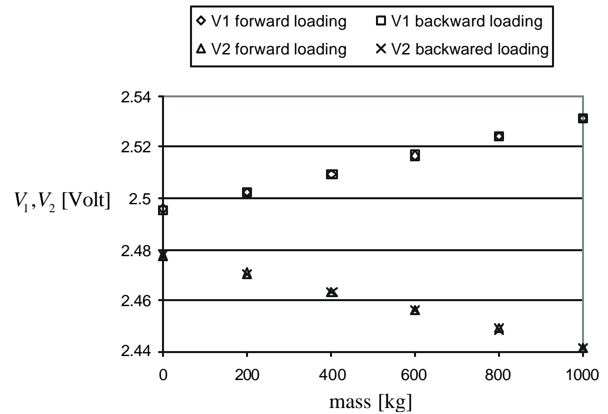

figure 18: Voltages across $R_1$ and $R_2$ as a function of mass (room temperature).

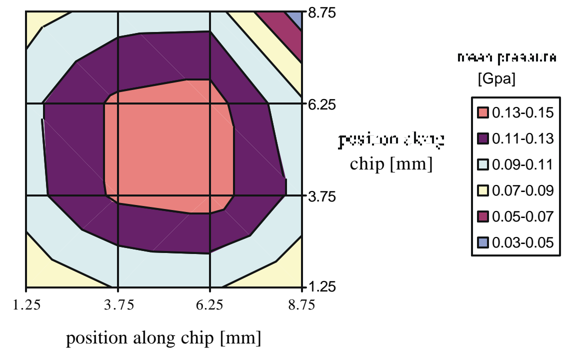

figure 19: Force distribution on the chip at 1000 kg (measured at 16 places).

## 8. Conclusions

The conclusions to be drawn from this investigation are:

- A piezoresistive 10 kN silicon force sensor was designed. New in the design is that it is made of silicon, the output is independent of the force distribution and it is compensated for the temperature coefficient of resistivity and for in-plane stretching and bending stresses in the chip and for common changes in zero load resistor values. The force distribution on the chip can be measured so that it can be detected whether the sensor has an oblique load or not.
- The chip with poly-Si strain gages was realized. The process is simple and robust.
- Hysteresis experiments were performed at four temperatures between 25 °C and 47 °C. The measurements at room temperature are in very close agreement with the finite element calculations. The maximum hysteresis error is within ±1.38 kg (±0.138 % of fso). Loading the chip five times tested creep. It follows that creep is smaller than 0.1 kg (0.01 % of the fso). However the non-repeatability in creep is ±0.35 kg (±0.035 % of the fso).
- It is believed that most of the hysteresis and non-repeatability in creep is caused by slip of the pressing blocks on gage 1. In order to reduce these effects it is proposed to bond a top wafer on top of gage 1.

## 9. References


[1] From product list of Flintec GmbH, Bahnhofstrasse 52-54, D-74909 Meckesheim, Bundesrepublik Deutschland. With kind permission of W. Vervure.

[2] K. Bethe, D. Baumgarten and J. Frank, Creep of sensor's elastic elements: metals versus non-metals, *Sensors and Actuators*, A21-A23:844-849, 1990.

[3] O. Sondergard and P. Gravesen, A new piezoresistive pressure transducer principle with improvements in media compatibility, *Journal of Micromechanics and Microengineering*, 6:105-107, 1996.

[4] K. Opperman, A new force sensor with metal measuring grid transverse to the line of force, *Sensors and Actuators*, A7:223-232, 1985.

[5] P.J. French, A.G.R. Evans, Polysilicon strain sensors using shear piezoresistance, *Sensors and Actuators*, 15:257-272, 1988.

[6] J. Suski, V. Mosser and J. Goss, Polysilicon SOI pressure sensor, *Sensors and Actuators*, A17:405-414, 1989.

[7] P.J. French and A.G.R. Evans, Piezoresistance in polysilicon and its applications to strain gauges, *Solid State Electronics*, 32:1-10, 1989.

[8] P.J. French and A.G.R. Evans, Piezoresistance in polysilicon, *Electronics Letters*, 20:999-1000, 1984.

[9] S.P. Timoshenko and J.N. Goodier, *Theory of elasticity*, McGraw-Hill International Editions, third edition, New York, ISBN 0-07-085805-5, 1970.

[10] J.J. Wortmans and R.A. Evans, Young's modulus in Silicon and Germanium, *Journal of Applied Physics*, 36:153-156, 1965.

[11] V.L. Spiering, Package stress reduction for micro-mechanical sensors: Application in a pressure sensor, *Ph.D. Thesis*, University of Twente, The Netherlands, 1994.

[12] K.E. Peterson, Silicon as a mechanical material, *Proceedings of the IEEE*, 70:420-457, 1982.

[13] V. Mosser, J. Suski, J. Goss and E. Obermeier, Piezoresistive pressure sensors based on polycrystalline silicon, *Sensors and Actuators*, A28:113-132, 1991.

[14] M.M. Mandurah, K.C. Saraswat, C.R. Helms and T.I. Kamins, Dopant segregation in polycrystalline silicon, *Journal of Applied Physics*, 51:5755-5763, 1980.

[15] E. Obermeier and P. Kopystynski, Polysilicon as a material for microsensor applications, *Sensors and Actuators*, A30:149-155, 1992.

[16] J. Binder, W. Henning, E. Obermeier, H. Schaber and D. Cutter, Laser-recrystallized polysilicon resistors for sensing and integrated circuits applications, *Sensors and Actuators*, A4:527-536, 1983.

[17] VLSI technology, S.M. Sze, McGraw-Hill, New York, ISBN 0-471-83704-0, 1988.

[18] N.H. Ditrick and M.S. Bae, An improved boron nitride glass transfer process, *Solid state Technology*, 23:69-73, 1980.

[19] P.J. French and A.G.R. Evans, Piezoresistance in polysilicon and its applications to strain gauges, *Solid State Electronics*, 32:1-10, 1989.

[20] C. Gui, Direct wafer bonding with chemical mechanical polishing, *Applications in sensors and actuators* (Ph.D. thesis), University of Twente, The Netherlands, 1998.